Line of Sight Calibration for Satellite Imagery Based on Matrix Detector

Guillaume Laurent[1], Alice Latourte[2], Fabrice Buffe[2], Bruno Vidal[2]

[1] Thales Services Numériques (TSN), 290 All. du Lac, 31670 Labège, France
[2] Centre National d’Etudes Spatiales (CNES), 18 avenue E. Belin, 31400 Toulouse cedex 9, France

Keywords: line of sight, auto-calibration, geometric refinement, sensor geometry, matrix sensor

Abstract

This study presents a self-calibration method for optical Earth observation satellites equipped with matrix sensors. Precise geolocation of each pixel in a satellite image requires accurate modelling of the acquisition geometry, typically achieved through refinement that corrects the geometry using measurements such as correspondences between image pixels and ground coordinates, or between pixels in different images.

A critical aspect of this modelling involves the sensor's internal geometry, which defines the line-of-sight (LOS) vector for each pixel in the focal plane. The calibration method proposed in this article eliminates the need for exogenous data (e.g., higher-resolution satellite images or airborne sensor imagery) by relying solely on a set of acquisitions in a specific configuration.

The method is evaluated and validated using CO3D imagery. Several evaluation criteria were developed for this purpose, including the reliability of the refinement process, the quality of tie-point intersections, inter-site result comparisons, and alignment with absolute references. This paper does not include the in-orbit performances due to confidentiality agreement.

1. Introduction

One of the crucial aspects of high-resolution optical satellite imagery is the ability to precisely locate each pixel on the ground. This is achieved through direct and inverse geolocation, establishing the following relationship and its inverse:

$$Ground\ Coordinates\ (\varphi, \lambda, h)\ \rightarrow Image\ Coordinates(i, j) \quad (1)$$

This relationship can be determined through physical modelling. Starting from the pixel position the image, a line of sight (LOS) is computed and intersected with the Earth at the desired altitude (constant or derived from a Digital Elevation Model, DEM).

Calibration of each pixel's position in the focal plane is necessary to obtain accurate geometric estimates. Initial ground-calculated models may prove insufficient, and satellite launches can modify acquisition geometry; therefore, this calibration must be performed in-flight through image analysis.

Most past and current missions utilize push-broom sensors with 1D linear arrays. Geometric calibration methods for these sensors typically involve image correlation to ground control points on super-sites of reference (Jacobsen, 2006), or employ endogenous methods such as "cross-mode" calibration (Delvit, 2012; Greslou, 2012) or the approach described by Yang (2018).

Matrix sensors are relatively recent additions to optical satellite imaging. Existing methods are unsuitable for these sensors because they require estimation of a bidirectional LOS model rather than the unidirectional model used for push-broom sensors. Methods based on Ground Control Points (GCPs) do not always provide sufficient accuracy, while two-image methods do not provide enough observables to decorrelate all geometric refinement parameters.

Self-calibration extends endogenous "cross-mode" calibrations by using a significantly larger set of input images to estimate two-dimensional LOS directions without ambiguity. A previous study (Vidal., 2022) tested this method on simulated data; it is here evaluated on real CO3D data.

2. Method

2.1 Geometric modeling of satellite acquisition: physical model and error sources

Geometric modeling associated with satellite acquisition enables the correlation between a pixel coordinate (i, j) and a ground coordinate expressed in a given geographic reference system such as WGS84 or UTM.
Each satellite has its own geometric model, which accounts for the satellite’s specific characteristics that influence the optical path for each pixel. Figure 1 provides a generic overview of this model: the coordinate (i, j) determines the timestamp and LOS direction in the local reference frame. The timestamp then provides the satellite’s attitude and position at the time of pixel (i, j) acquisition, allowing the LOS direction to be transformed into the ITRF reference frame and intersected with an Earth model.

Errors can arise at each stage of geometric modelling, including:

- Inaccuracies in focal plane mapping
- Pixel timestamping errors
- Satellite attitude and position uncertainties
- Earth model intersection errors

These errors collectively degrade the localization model. This study focuses specifically on focal plane mapping errors, which primarily stem from the instrument's optics:

- Imprecise knowledge of the focal length leads to magnification errors.

- Optical path variations where each image pixel passes through different portions of the mirror, introducing both global and local distortions in LOS directions (Figure 2).

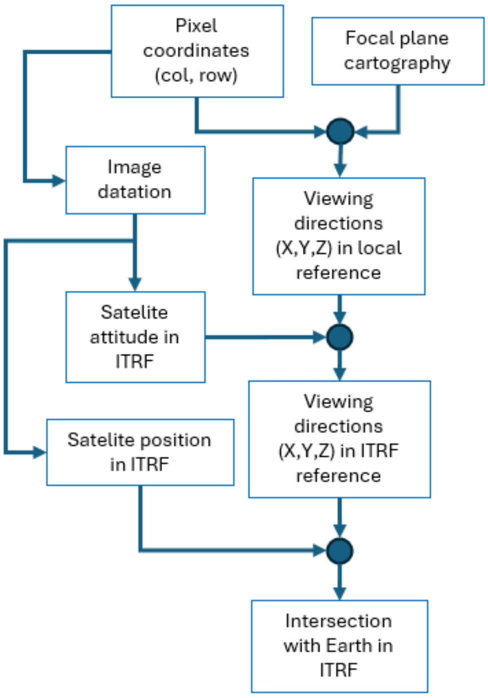

Figure 1: Generic satellite geometric modeling

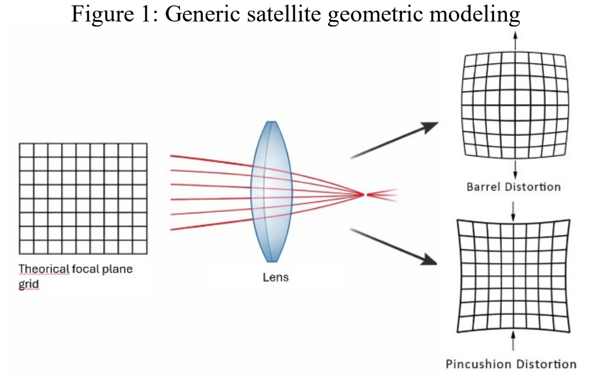

Figure 2: Lens inducing distortions in the focal plane mapping

2.2 Principle of refinement: parameter optimization from observations

Refining a geometric model involves adjusting the model to align with real-world measurements. These measurements can take two forms:

- Ground Control Points (GCPs): A relationship between a pixel in an image and a ground location
- Tie Points (TPs): A relationship between multiple images where pixel (i, j) in Image 0 corresponds to pixel (k, l) in Image 1 and pixel (y, z) in Image N

These relationships can be established through manual pointing or automatic correlation techniques (e.g., SIFT descriptors or template matching).
A GCP provides an absolute constraint: the LOS must pass through a fixed ground point. A TP offers a relative constraint: the LOS of corresponding pixels across N images must intersect. Generally, higher values of N provide more information for refinement. The configuration of intersecting image acquisitions also significantly impacts the information contributed by these relationships.

2.3 Dense correlation between images to obtain multi-image TPs

TPs required for calibration are calculated on a dataset of images specifically acquired for calibration. The goal is to achieve maximum correspondence between the different viewing directions of the matrix. The multiplicity defines the number of images that a TP connects. The higher this multiplicity, the more information the TP will provide.

The images are therefore acquired by optimizing both the diversity of overlap between images and the maximum number of overlapping images in each area.

The calculation of the TPs is performed in 3 steps:

- Reprojection of the secondary image onto the geometry of the reference image
- Dense NCC between the two images
- Colocalization of the shift found in the geometry of the secondary image

To calculate the reprojection-correlation combinations to be performed, an iterative intersection calculation is carried out. The intersections are calculated first in pairs, then in groups of three, and so on, up to N by N.

Figure 3 illustrates the process: on the left is the extent of the 5 images, and on the right are the 20 correlation zones maximizing the multiplicity. Within each zone, one image is chosen as the reference, and all the others are declared secondary and reprojected/correlated to the reference. This ensures the extraction of the maximum amount of information from these intersections.

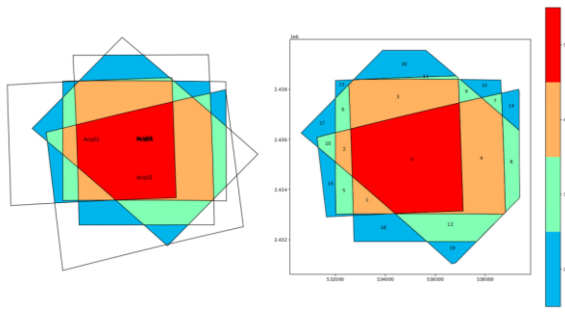

Figure 3: Footprint of 5 images and associated correlation zones (multiplicity is represented by color)

2.4 Optimisation

The geometric refinement involves minimization using the Levenberg-Marquardt algorithm. The function to be minimized is:

$$cost = F_{costTP} + F_{costGCP} + F_{costParameters} \quad (2)$$

For TP, the cost function is:

$$F_{costTP} = \sum_{i=1}^{N} \sum_{j \in I_i} \frac{m_{ij} - \widehat{m_{ij}}(\theta)}{p_{ij}} \quad (3)$$

where

N = total number of TP
I_i= set of images in which the TP is visible
m_{ij}= provided measure of the TP i in the image j
$\widehat{m_{ij}}(\theta)$ = estimated measure of the TP i in the image j for optimization of parameter θ
p_{ij} : provided image precision of the TP i in the image j

This relates to the difference between the measured image position and the estimated image position from minimization, for each LOS. A ground intersection can also be provided to add a constraint, such as altitude derived from an external DEM.

For Ground Control Points (GCP), the cost function is:

$$F_{costGCP} = \sum_{i=1}^{N} \frac{m_i - \widehat{m_i}}{p_i} + \frac{g_i - \widehat{g_i}}{q_i} \quad (4)$$

where

N = total number of GCP
m_i= provided image measure of the GCP i
$\widehat{m_i}(\theta)$ = estimated image measure of the GCP i for optimization of parameter θ
p_i = provided image precision of the TP i
g_i= provided ground measure of the GCP i
$\widehat{g_i}(\theta)$ = estimated ground measure of the GCP i for optimization of parameter θ
q_i = provided ground precision of the GCP i

This cost function measures the discrepancy between the observed ground location of the GCP and the location predicted by the geometric model, ensuring that the refinement process aligns the model with absolute ground truth data.

For the parameters, the cost function is:

$$F_{costParameters} = \sum_{i=1}^{N} \frac{\left(\theta_i - \widehat{\theta_i}\right)}{p_i} \quad (5)$$

where

N = total number of parameters
θ_i= initial value of the parameter i
$\widehat{\theta_i}$ = estimated value of the parameter i
p_i = provided precision of the parameter i

This cost function ensures that the refinement process respects the initial estimates of the parameters and their associated uncertainties, preventing excessive deviations that could lead to unrealistic or unstable solutions.

The optimization is performed three times, with filtering at each iteration to eliminate outliers. This filtering calculates a score (e.g., Z-Score or MAD) for each TP or GCP, and deactivates measurements that exceed a certain threshold.

Once optimization is complete, covariance and correlation matrices are computed by inverting the Jacobian. These matrices provide valuable information about the geometric refinement:

- Reliability of parameter estimates
- Correlation between parameters.

2.5 Self-calibration of LOS directions

2.5.1 Definition of parameters to optimize

To model focal plane mapping errors, two-dimensional polynomials are employed. These polynomials effectively capture both radial distortions and higher-order local effects on the focal plane.

$$x_{corrected} = x + \begin{pmatrix} K_{00}x^0y^0 & K_{10}x^1y^0 & \cdots & K_{n0}x^ny^0 \\ K_{01}x^0y^1 & K_{11}x^1y^1 & \dots & K_{n1}x^ny^1 \\ \vdots & \vdots & \ddots & \vdots \\ K_{0n}x^0y^n & K_{1n}x^1y^n & \cdots & K_{nn}x^ny^n \end{pmatrix}$$

$$y_{corrected} = y + \begin{pmatrix} L_{00}x^0y^0 & L_{10}x^1y^0 & \cdots & L_{n0}x^ny^0 \\ L_{01}x^0y^1 & L_{11}x^1y^1 & \dots & L_{n1}x^ny^1 \\ \vdots & \vdots & \ddots & \vdots \\ L_{0n}x^0y^n & L_{1n}x^1y^n & \cdots & L_{nn}x^ny^n \end{pmatrix} \quad (6)$$

The refinement process optimizes the values of matrices K and L, each of size NxN. This effectively adds a 2D polynomial of order N to the LOS, including all cross terms between X and Y.

To ensure numerical stability, it is crucial to normalize the x and y positions. Using a high-order polynomial without normalization can result in values spanning several orders of magnitude, leading to a poorly conditioned problem and potential optimization failure.

$$x_{inter} = x - \min(x)$$

$$half\_range_x = \frac{max(x_{inter})}{2}$$

$$x_{normalized} = \frac{(x_{inter} - half\_range_x)}{half\_range_x} \quad (7)$$

This normalization obtains coordinates (x, y) between -1 and 1, providing good conditioning for optimization.

An attitude bias is also corrected for each satellite, as the images may initially be poorly registered with each other.

The attitude bias is applied just before switching from the satellite reference frame to the ITRF reference frame, and it is applied as follows:

$$viewingDir_{ITRF} = R_{sat\rightarrow ITRF}.R_{global}.viewingDir_{sat} \quad (8)$$

where

$$R_{global} = R_{roll}.R_{pitch}.R_{yaw}$$

$$R_{roll} = \begin{pmatrix} 1 & 0 & 0 \\ 0 & \cos(\alpha) & -\sin(\alpha) \\ 0 & \sin(\alpha) & \cos(\alpha) \end{pmatrix}$$

$$R_{pitch} = \begin{pmatrix} \cos(\beta) & 0 & \sin(\beta) \\ 0 & 1 & 0 \\ -\sin(\beta) & 0 & \cos(\beta) \end{pmatrix}$$

$$R_{yaw} = \begin{pmatrix} \cos(\gamma) & -\sin(\gamma) & 0 \\ \sin(\gamma) & \cos(\gamma) & 0 \\ 0 & 0 & 1 \end{pmatrix}$$

3. Results

The performance and results obtained during the calibration of the satellites are unfortunately not disclosable. Only the description of the input data, analysis methods, and algorithm adaptations for CO3D will be presented in this study. The LOS calibration is interdependent with the calibration of many other satellite calibrations, which are fully described in (Buffe, 2026).

It is necessary to have a circular error in the LOS of less than 0.1 pixel on 90% of the matrix pixels (0.1 pixels @ CE90), as this directly impacts the accuracy of the digital spatial models subsequently produced by stereoscopy. The previous study (Vidal, 2022) showed (by application to simulated data) that this performance could be achieved.

3.1 CO3D calibration site

The agility of CO3D satellites enables acquisition of 9 views at each calibration site per pass. In two passes, the dataset required for LOS refinement can be obtained.

These two passes must be as close in time as possible to obtain the highest quality correlations. Pre-calibration radiometric calibration of the satellites is necessary because an acquisition with an out-of-focus instrument correlate poorly with an in-focus equivalent (Figure 4). CO3D radiometric calibration is described in detail in (Lucas, 2026)

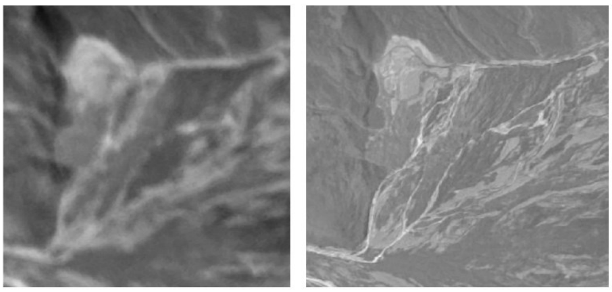

Figure 4: CO3D Atacama acquisition before (left) and after (right) refocus

Acquisitions taken over too large a time interval exhibit different shadows (Figure 5).

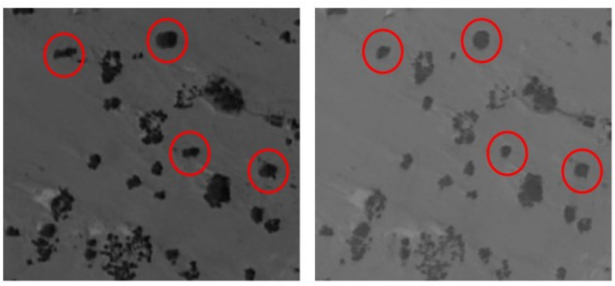

Figure 5: CO3D China acquisition in October (left) and January (right).

Approximately ten calibration sites (Table 1) were selected based on the following criteria:

- Flat relief
- Few buildings
- A landscape suitable for correlation (fixed structure in the image)
- Ease of acquisition and revisit

	CO3D1	CO3D2	CO3D3	CO3D4
ATACAMA	8	9	8	6
LA SILLA	11	12	8	7
NEVADA	4	6	4	5
CHINA	3	4	6	4
OMAN	9	8	4	7
CASA DE PIEDRA	2	3	6	5
AUSTRALIA 1	2	3	5	5
AUSTRALIA 2	3	2	3	4
KARAKOUM	4	3	2	3

Table 1: number of datasets (set of 9 acquisitions) for each LOS calibration sites / satellite

3.2 Pseudo-intersection performance

For each calibration site, the LOS correction can first be estimated by analysing the pseudo-intersections. The pseudo-intersection is the 3D point that minimizes the following function:

$$E(X) = \sum_{i=1}^{N} ||(I - u_i {u_i}^T)(X - P_i)||^2 \quad (9)$$

where

u_i = viewing direction vector for measure i
P_i = viewing direction origin for measure i
I = 3x3 identity matrix
X = pseudo-intersection point

The residual of this minimization gives the deviation of each LOS from the pseudo-intersection point, reflecting the quality of intersection for each TP. Statistical and spatial analysis (Figure 6) therefore allows identification of any potential defects in the geometric correction.

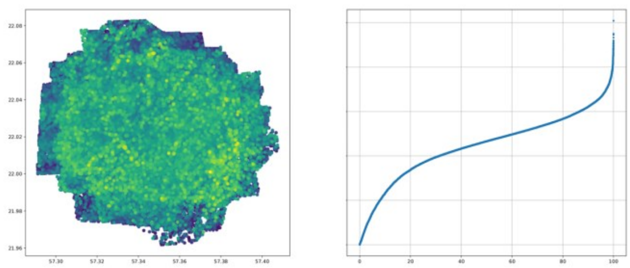

Figure 6: 2D radius pseudo-intersections and their cumulative distribution

The altitude of these pseudo-intersections is also a criterion; it can be compared to an altimetric reference to ensure that the solution does not deviate excessively. Figure 7 shows a comparison with the Copernicus DEM, which has an altitude precision of 4 meters. A solution would be invalid if it exceeded this value.

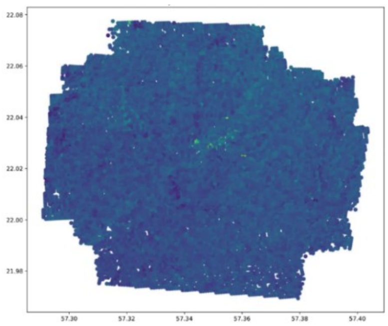

Figure 7: Distance between pseudo-intersections and Copernicus DEM

3.3 Co-registration check

In parallel with statistical analysis, a co-registration analysis is necessary. Initially, it is possible to verify the co-registration of the N images in the dataset by reprojecting them onto a common geometry (geometry of one of the images or orthorectification onto a UTM grid). This method does not require exogenous data and allows easy detection of poor optimization parameter settings. Visual analysis (Figure 8) or correlation analysis (Figure 9) is performed.

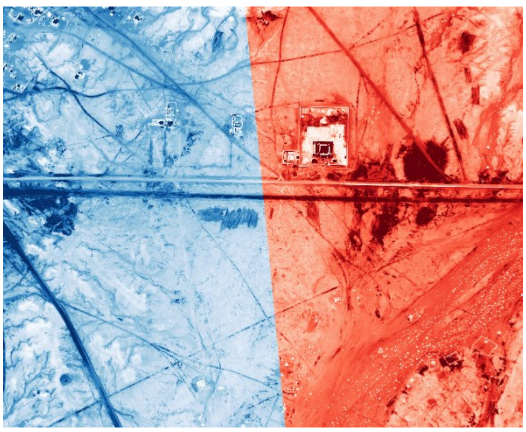

Figure 8: CO3D 1 (blue) and 2 (red) co-registered images

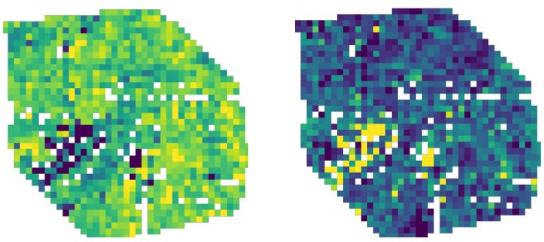

Figure 9: columns (left) and lines (right) residual shifts between co-registered, obtained by NCC correlation

Similarly, it is possible to correlate the corrected images with a higher-resolution absolute reference that has already been calibrated, such as PCRS aerial imagery or satellite imagery like Pléiades Neo. However, the estimation of co-registration quality may be degraded by DEM errors or attitude modelling errors, and will be limited by the quality of the reference itself.

3.4 Correlation / Covariance matrix of parameters

Analysis of correlation and covariance matrices allows us to assess the suitability of a configuration.

Tests on simple configurations help us better understand the contribution of each image to self-calibration.

The main uncertainty during LOS refinement stems from the epipolar orientation of the images relative to each other. Images acquired on the same satellite track generate LOS inscribed on the epipolar plane (Figure 10).

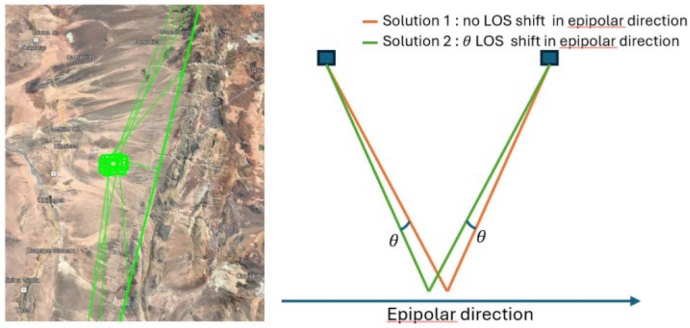

Figure 10: Acquisition configuration on Atacama and multiple solution for LOS calibration in epipolar direction

The accuracy of the LOS will therefore be degraded in this direction.

A refinement using two column-shifted images (Figure 11) demonstrates this effect. Looking at the covariance of the refined variables (Figure 12), we observe that the polynomial correcting the X direction is less accurately estimated; it is the direction almost aligned with the epipolar axis (within the orbital inclination, i.e., 7°).

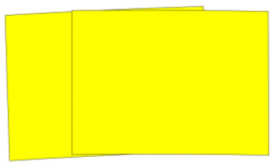

Figure 11: 2 images auto-calibration case with shifted longitude location

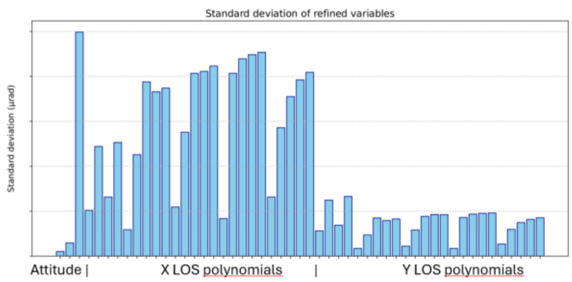

Figure 12: Parameters covariance for auto-calibration with 2 images

With the use of an image at a 90° angle to the central image (Figure 13), this uncertainty on the epipolar direction is removed: the epipolar direction is found on the Y axis for the rotated image

https://doi.org/10.5194/isprs-archives-XLIX-B1-2026-271-2026 |

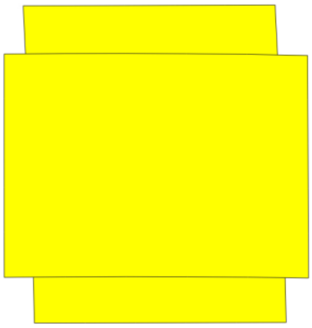

Figure 13: 2 images auto-calibration case with different heading

The covariances of the parameters for this case (Figure 14) confirm that the reliability of the correction polynomials in X is similar to that in Y.

.

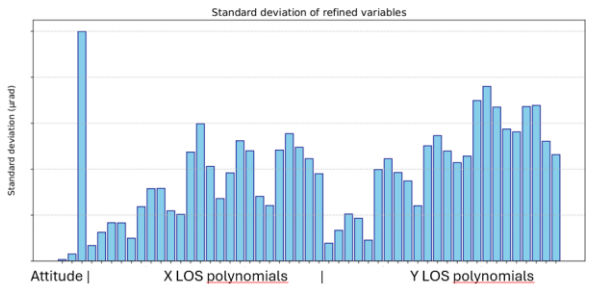

Figure 14: Parameters covariance for auto-calibration with 1 heading 90° image

The operational configuration is therefore deduced from these observations and operational constraints: 9 images can be acquired at each pass, Figure 15 shows a configuration allowing to obtain TPs linking different parts of the focal plane, which will improve the minimization.

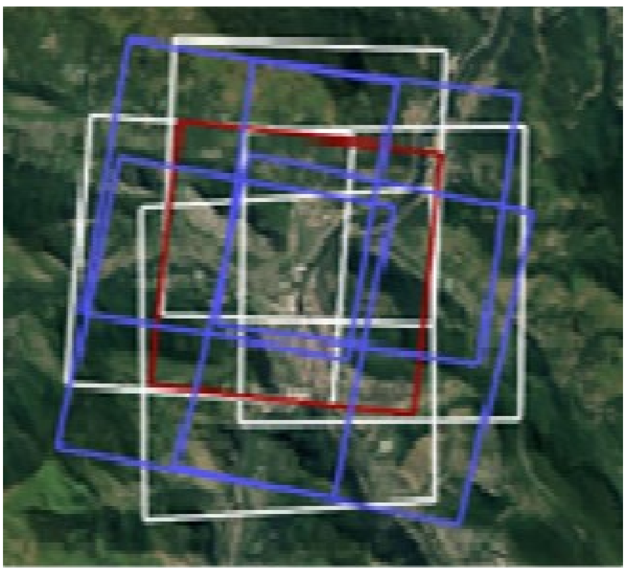

Figure 15: 9 images auto-calibration configuration

Nine additional images taken on a different passage, with the heading rotated 90°, complete the dataset. Figure 16 shows the overlap between images in this case, with up to 18 scenes intersecting at the center.

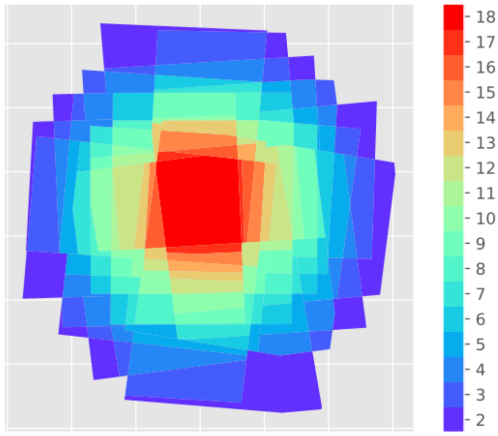

Figure 16: overlapping between images for complete auto-calibration case (18 images)

The correlation matrix (Figure 17) for the case of complete self-calibration provides valuable insights.

1. Roll/Pitch correlation: The roll and pitch parameters exhibit strong mutual correlation. This is expected, as an offset in roll or pitch for one image necessitates corresponding adjustments in the others to preserve the intersections of tie points (TPs).

2. Yaw correlation: The yaw parameters are also strongly correlated. This makes sense, as a uniform rotation across all images would not alter the solution.

3. Magnification and LOS correlation: The magnification and LOS parameters are correlated with each other and with the attitude parameters. This suggests that the second-order polynomials used to correct the LOS can model a magnification effect, and the estimated magnification is influenced by the acquisition conditions.

However, self-calibration cannot independently correct magnification. The quality of the LOS intersections remains unchanged regardless of the magnification applied to the images. Only exogenous data introduced into the optimization process—such as ground control points (GCPs) or altitude data derived from a digital elevation model (DEM)—can constrain and refine the scaling value. However, the current approach has limited precision; more accurate methods for estimating magnification must be explored.

4. Focal Plane Polynomials: A checkerboard pattern of correlation and anti-correlation is observed in the polynomial parameters of the focal plane, separately for the X and Y directions.
These correlations arise from the use of non-orthogonal basis polynomials. Specifically, monomials of even powers are correlated with each other, as are monomials of odd powers. This issue could be addressed by employing orthogonal basis polynomials, such as Legendre or Chebyshev polynomials. While this approach was not tested in the current study, it warrants further investigation for potential validation.

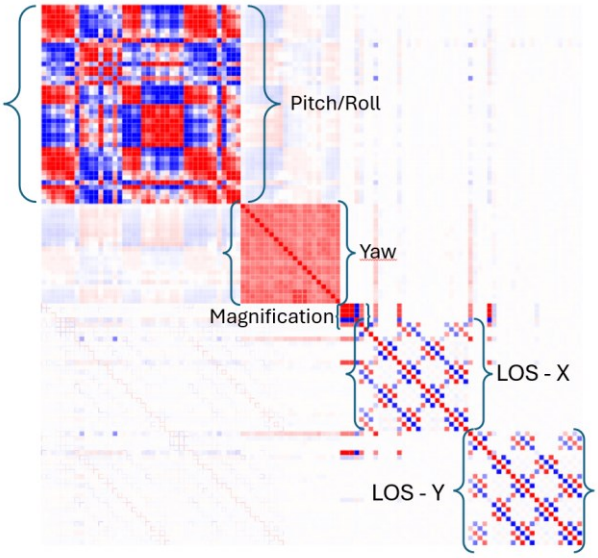

Figure 17: Correlation matrix for a complete auto-calibration dataset

Analysis of the covariances of the X and Y parameters of the LOS also shows good reliability of estimation.

3.4.1 Inter-site performance: One of the most important performance criteria is inter-site comparison. Refinements are performed on several datasets, median refined LOS directions are calculated, and CE90 performance is computed between the median and each site (Figure 18).

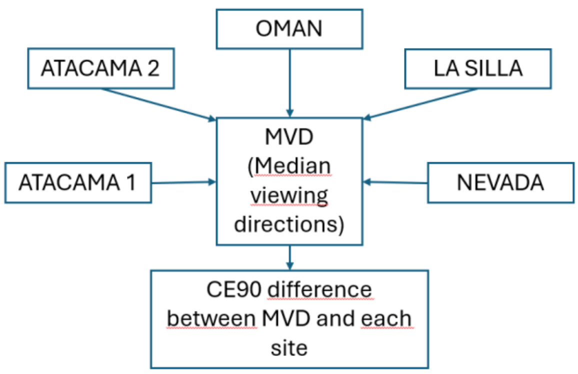

Figure 18: Inter-site comparison method

A pre-alignment of LOS directions, accounting for rotation and magnification, is performed before calculation. Since focal plane rotation is equivalent to a satellite yaw error, it cannot be estimated. Magnification may vary for each site (due to satellite positioning errors or thermo-elastic effects altering focal length), making it irrelevant to include in performance estimation. Instead, its value and variability are estimated separately.

This pre-alignment is achieved through a pseudo-affine process:

- A single arbitrary imaging model is duplicated, with each duplicate assigned the LOS of a satellite.
- TPs are created between the N models on a regular grid, connecting the images as follows:

$$for\ i\ in\ 0 \ldots ncol\ and\ j\ in\ 0 \ldots nlig:$$
$$im1(i,j) \leftrightarrow im2(i,j) \ldots \leftrightarrow imN(i,j) \quad (10)$$

- Each model undergoes refinement for yaw rotation and scaling (order 0 of the focal plane along the Z-axis). These variables are adjusted to ensure that the calculated LOS across all sites align as closely as possible.
- The refined yaw rotation and scaling are then integrated into the LOS of each model.

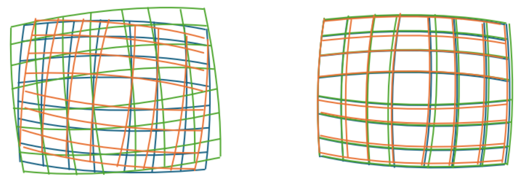

Figure 19: LOS for each site before (left) and after (right) rotation and magnification adjustment

Once the LOSs are aligned (Figure 19), statistics are calculated, along with a difference graph per sub-zone (Figure 20). This graph shows where the greatest inter-site differences lie. Here, we see that these are the matrix edges where the difference is greatest, and therefore where the LOSs are least accurately estimated.

Figure 20: inter-site difference of aligned LOS (one color per site)

3.4.2 Magnification calibration: Since the self-calibration method could not reproduce the magnification value, two additional methods were implemented to estimate it.

- Estimation by SRP residual

By retrieving the CO3D image registration results using SRP (Erblang, 2026), it is possible to extract the magnification component from the refinement residues (Figure 21). This component, averaged over several hundred images, provides a good indication of the average magnification.

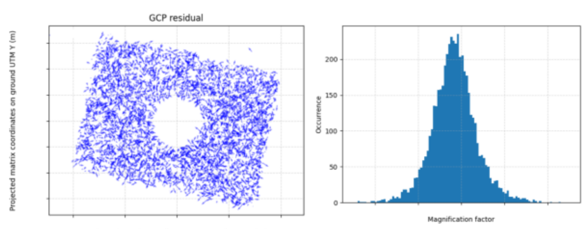

Figure 21: Magnification estimation by SRP residual statistics

This contribution has been peer-reviewed.
https://doi.org/10.5194/isprs-archives-XLIX-B1-2026-271-2026

- Estimation by lever arm

The second method also uses SRP control points, but multiplies their accuracy by a lever arm (the initial georeferencing accuracy of the SRPs being insufficient to estimate the magnification at the expected performance level). The configuration shown in Figure 22 allows the effect of magnification to be cumulative 14 times across the entire series. The images are correlated with each other and with the SRPs. Any magnification error will therefore impact the GCPs located on the first and last acquisitions by a factor of 14.

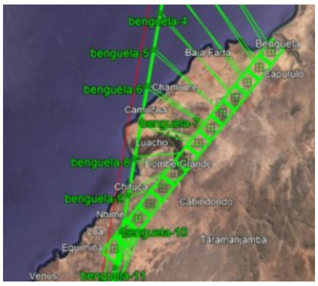

Figure 22: **Acquisition series of 14 images maximizing magnification measurement sensitivity**

Comparing the results between the two methods allows us to estimate their reliability.

4. Conclusions

This method has proven suitable for calibrating CO3D satellites, with a few specific adaptations. The performance metrics developed have provided confidence in the self-calibration results produced at the various sites.

One remaining issue is the non-orthogonality of the polynomials used for LOS correction, which creates parameter correlations and hampers algorithm convergence.

In the context of CO3D, joint minimization should be tested, as the altimetric reconstruction performance is highly dependent on the inter-satellite calibration of each stereoscopic pair. It would be worthwhile to investigate a 36-image minimization that optimizes the LOS of each pair simultaneously.

5. References

Jacobsen, K. (2006). Calibration of optical satellite sensors. In *Proceedings of the International Calibration and Orientation Workshop EuroCOW*.

Vidal, B., Laurent, G., Buffe, F., Binet, R., Zanga, W., & Greslou, D. (2022). Line of Sight Auto-Calibration for CO3D Rolling Shutter Matrix Detector. *The International Archives of the Photogrammetry, Remote Sensing and Spatial Information Sciences*, *43*, 107-112.

Yang, B., & Pi, Y. (2018). Independent On-Orbit Geometric Calibration of Optical Satellite Based on Weighted Virtual Observation. The International Archives of the Photogrammetry, Remote Sensing and Spatial Information Sciences, 42, 461-467.

Greslou, D., De Lussy, F., Delvit, J. M., Dechoz, C., & Amberg, V. (2012). Pleiades-HR innovative techniques for geometric image quality commissioning. *The International Archives of the Photogrammetry, Remote Sensing and Spatial Information Sciences*, *39*, 543-547.

F. Buffe, S. Lucas, A. Latourte, N. Delaygue T. Accadia, D. Youssefi, A. Dick, C. Luitot, M. Bruno, C. Coggiola, Y. Tanguy, L. Lebègue, C. Thomas, M. Schillinger, A. Chambrelan (2026). CO3D Image quality calibration, ISPRS 2026, Toronto

Delvit, J. M., Greslou, D., Amberg, V., Dechoz, C., de Lussy, F., Lebegue, L., ... & Bernard, L. (2012). Attitude assessment using Pleiades-HR capabilities. *The International Archives of the Photogrammetry, Remote Sensing and Spatial Information Sciences*, *39*, 525-530.

M. Erblang, E. Saulnier , G. Laurent, N. Delaygue, F. Buffe, A. Latourte, M. Jassaud, N. Bricout (2026). Global Block Adjustment for Mosaicked Stereoscopic Satellite Imagery, ISPRS 2026, Toronto

S. Lucas, O. Amram, C. Latry, C. Thomas, M. Schillinger (2026). Radiometric features and ground processing for high-resolution Earth observation satellite Bayer matrix-based images like CO3D, ISPRS 2026, Toronto